

NUMERICAL CALCULATION OF SEICHE MOTIONS IN HARBOURS
OF ARBITRARY SHAPE

P. Gaillard
Sogreah, Crenoble, France

ABSTRACT

A new method of calculation of wave diffraction around islands, offshore structures, and of long wave oscillations within offshore or shore-connected harbours is presented. The method is a combination of the finite element technique with an analytical representation of the wave pattern in the far field. Examples of application are given, and results are compared with other theoretical and experimental investigations.

INTRODUCTION

The prediction of possible resonant response of harbours to long wave excitation may be an important factor at the design stage. Hydraulic scale models have the disadvantage of introducing some bias in the results due to wave reflection on the wave paddle and on the tank boundaries. Numerical methods on the other hand can avoid such spurious effects by an appropriate representation of the unbounded water medium outside the harbour.

Various numerical methods exist for calculating the seiche motions in harbours of arbitrary shape and water depth configuration. Among these, the hybrid-element methods, as described by Berkhoff [1], Bettess and Zienkiewicz [2], Chen and Mei [3], Sakai and Tsukioka [8] use a combination of the finite element technique with other methods for representing the velocity potential within the harbour and in the offshore zone. This paper presents a new method based on the same general approach, with an analytical representation of the wave pattern in the far field. It differs from the former methods in several aspects stressed hereafter.

We consider here two kinds of applications:

- a) the first is the study of wave diffraction by islands or bottom seated obstacles in the open sea and the study of wave oscillations within and around an offshore harbour.
- b) the second is the study of wave oscillations within a shore-connected harbour with a totally reflective coastline, which is assumed rectilinear beyond a certain distance.

BASIC EQUATIONS

The numerical calculation of long period water oscillations in harbours of arbitrary shape and bottom configuration is based on the linear shallow water wave equation for an inviscid fluid:

$$\nabla \cdot [h \nabla \zeta] - \frac{1}{g} \zeta_{tt} = 0 \tag{1}$$

where $\zeta(x,y,t)$ is the water surface elevation above mean sea level,
 $h(x,y)$ is the water depth distribution,
 g the acceleration due to gravity.

The numerical models based on the present method include two domains:

- in a bounded region D_1 including the harbour and the vicinity of the harbour entrance, the water depth is defined according to the bottom topography on the site studied, and a finite element technique is used for solving the above equation.
- In the outer region D_2 , extending to infinity, and bounded by an unlimited rectilinear reflecting coastline in the case of a shore-connected harbour, the water depth is assumed constant, equal to h_0 , and an analytical solution of (1) is used in the form of a finite series expansion.

The boundary C_{12} interconnecting both domains is either a full circle in the case of an island-type harbour or structure, or a half circle in the case of a shore-connected harbour, as shown in figure 1.

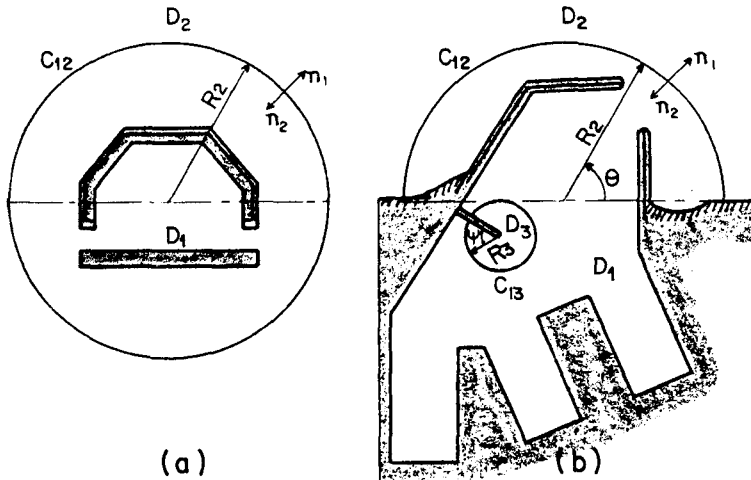


Fig.1 Definition sketch: (a) offshore case ; (b) nearshore case

A periodic excitation by a plane incident wave of arbitrary direction α , frequency f (or angular frequency ω) and height $2a_0$ is taken as input to the model at infinity and the steady-state dynamic response of the model is calculated. A variable frequency scanning technique is used to detect the resonant modes.

We thus reduce the problem to seeking, for a finite number of wave angular frequencies ω , a complex function of space $\bar{\zeta}(x,y)$ such that:

$$\zeta(x,y,t) = \text{Re} \{ \bar{\zeta}(x,y) \exp(-i\omega t) \} \quad (2)$$

This function is a solution of the Helmholtz equation:

$$\nabla \cdot [h \nabla \bar{\zeta}] + \frac{\omega^2}{g} \bar{\zeta} = 0 \quad (3)$$

We shall refer to the solutions of (3) in D_1 and D_2 as $\bar{\zeta}_1$ and $\bar{\zeta}_2$ respectively. The boundary conditions imposed on these solutions are as follows:

$$\frac{\partial \bar{\zeta}}{\partial n} = 0 \quad \text{on } C_{SB} \quad (4)$$

$$\bar{\zeta}_1 = \bar{\zeta}_2 \quad \text{on } C_{12} \quad (5)$$

$$\frac{\partial \bar{\zeta}_1}{\partial n_1} = - \frac{\partial \bar{\zeta}_2}{\partial n_2} = G_{12}(\theta)$$

$$\bar{\zeta}_2 \rightarrow \bar{\zeta}_A \quad \text{for } r \rightarrow \infty \quad (6)$$

The first condition expresses that waves are totally reflected from all solid boundaries i.e. harbour structures and coastline. This assumption is generally valid as wave steepness is low for the periods considered.

The set of conditions (5) express the continuity of the water surface elevation and of the horizontal velocities at the common boundary C_{12} .

The last condition imposes the behaviour of the solution in the far field, behaviour which depends on the type of application considered.

In the case of an offshore harbour or structure $\bar{\zeta}_A$ is representative of the plane incident wave, which can be expressed, in polar coordinates (r,θ) with the origin at the centre of C_{12} , as:

$$\bar{\zeta}_A = \bar{\zeta}_i = a_0 \sum_{n=0}^{\infty} \epsilon_n (i)^n J_n(kr) \cos n(\theta - \alpha) \quad (7)$$

with: $i = \sqrt{-1}$

J_n = the Bessel function of order n

k = the wave number associated with frequency ω by:

$$k = \omega(gh_0)^{-1/2} \tag{8}$$

$$\epsilon_n = \begin{cases} 1 & n=0 \\ 2 & n \geq 1 \end{cases} \tag{9}$$

In the case of a shore-connected harbour, $\bar{\zeta}_A$ is representative of the superposition of the incident waves and of their reflection on the coastline, which is considered as totally reflective. Taking the origin of along the shoreline, $\bar{\zeta}_A$ is expressed as:

$$\bar{\zeta}_A = 2a_0 \sum_{n=0}^{\infty} \epsilon_n (i)^n J_n(kr) \cos n\alpha \cos n\theta \tag{10}$$

The solution in D_2 is consequently split into two components $\bar{\zeta}_A$ and $\bar{\zeta}_D$, where $\bar{\zeta}_D$ is representative of the diffracted waves due to the presence of the harbour or of the isolated structure under consideration. These waves radiate outward from the latter to infinity, and thus should satisfy Sommerfeld's radiation condition:

$$\lim_{r \rightarrow \infty} \left\{ \sqrt{r} \left[\frac{\partial \bar{\zeta}_D}{\partial r} - ik \bar{\zeta}_D \right] \right\} = 0 \tag{11}$$

VARIATIONAL FORMULATION

The solution of the problem is obtained through a variational approach, which is briefly described here. Considering first the two domains independently and the function $G_{12}(\theta)$ in (5) as a given boundary condition, the solution in D_1 is ascribed to make stationary the functional:

$$F_1(\zeta) = \frac{1}{2} \iint_{D_1} \left[h(\nabla\zeta)^2 - \frac{\omega^2}{g} \zeta^2 \right] ds - \int_{C_{12}} h \zeta_1 G_{12} d\sigma \tag{12}$$

and the solution in D_2 is associated with the functional:

$$F(\zeta) = -\frac{1}{2} \iint_{D_2} \left[\nabla \cdot (h\nabla\zeta) + \frac{\omega^2}{g} \zeta \right] \zeta ds + \int_{C_{12}} h \left[\frac{1}{2} \frac{\partial \zeta}{\partial n} + G_{12} \right] \zeta d\sigma \tag{13}$$

Since ζ_2 is represented in an analytical form which satisfies a priori equation (3), the first integral in (13) actually vanishes.

If we now consider G_{12} as an unknown function, our objective is to make stationary, for any first variation of ζ_1 , ζ_2 and G_{12} , the functional resulting from the addition of (12) and (13), i.e.:

$$F(\zeta) = \frac{1}{2} \iint_{D_1} \left[h(\nabla\zeta)^2 - \frac{\omega^2}{g} \zeta^2 \right] ds + \frac{1}{2} \int_{C_{12}} h \frac{\partial \zeta_2}{\partial n_2} \zeta_2 d\sigma + \int_{C_{12}} h G_{12} (\zeta_2 - \zeta_1) d\sigma \tag{14}$$

G_{12} is a periodic function of θ , which can be represented, in the case of an offshore structure, by a Fourier series expansion with unknown coefficients C_{1m} , C_{2m} . The requirement of stationarity of (14) for arbitrary first variations of these coefficients, leads to the following conditions:

$$\int_{C_{12}} (\zeta_2 - \zeta_1) \begin{Bmatrix} \cos m\theta \\ \sin m\theta \end{Bmatrix} d\theta = 0 \quad m = 0, 1, 2, \dots \quad (15)$$

When these conditions are satisfied, the last boundary integral of (14) vanishes.

In the case of a shore-connected harbour, $G_{12}(\theta)$ is an even function of θ . In this type of application, only those conditions in (15) involving $\cos m\theta$ are necessary.

The above functional can be represented in terms of the complex function $\bar{\zeta}$ by insertion of (2). It then appears as a function of time of the form:

$$F(\zeta) = \frac{1}{4} \operatorname{Re} \left\{ F_c(\bar{\zeta}) + F_v(\bar{\zeta}) \exp(2i\omega t) \right\} \quad (16)$$

$$F_c(\bar{\zeta}) = \iint_{D_1} \left[h \nabla \bar{\zeta}_1 \cdot \nabla \bar{\zeta}_1^* - \frac{\omega^2}{g} \bar{\zeta}_1 \bar{\zeta}_1^* \right] ds + \int_{C_{12}} h \frac{\partial \bar{\zeta}_2}{\partial n_2} \bar{\zeta}_2^* d\sigma \quad (17)$$

$$F_v(\bar{\zeta}) = \iint_{D_1} \left[h (\nabla \bar{\zeta}_1^*)^2 - \frac{\omega^2}{g} (\bar{\zeta}_1^*)^2 \right] ds + \int_{C_{12}} h \frac{\partial \bar{\zeta}_2^*}{\partial n_2} \bar{\zeta}_2^* d\sigma \quad (18)$$

where $\bar{\zeta}^*$ is the complex conjugate of $\bar{\zeta}$.

The values of $\bar{\zeta}_2$ and of its normal derivative along C_{12} depend on the values of $\bar{\zeta}_1$ on this boundary, through the conditions (15). Consequently, the values of $\bar{\zeta}_1$ at N arbitrarily chosen nodes within D_1 and on its boundary constitute a complete set of independent degrees of freedom of the functionals F and F_v . By expressing F_c and F_v in terms of these variables, it can be shown that:

$$\frac{\partial F_v}{\partial \bar{\zeta}_1^*} = \left(\frac{\partial F_c}{\partial \bar{\zeta}_1} \right)^* \quad (19)$$

In view of this property, the stationarity of $F(\zeta)$ is ensured at any time t when:

$$\frac{\partial F_c}{\partial \bar{\zeta}_{1n}^*} = 0 \quad n = 1, 2, \dots, N \quad (20)$$

SOLUTION FOR AN OFFSHORE HARBOUR OR STRUCTURE

In the offshore case, in which C_{12} is a full circle, the solution in domain D_2 involves the following series expansion of $\bar{\zeta}_D$:

$$\bar{\zeta}_D(r, \theta) = \sum_{m=0}^{\infty} H_m^{(1)}(kr) \left[\bar{\omega}_{1m} \cos m\theta + \bar{\omega}_{2m} \sin m\theta \right] \quad (21)$$

where $H_m^{(1)}$ is the Hankel function of the first kind and of order m .

The insertion of (21) into (15) leads to:

$$\begin{cases} \bar{\omega}_{1m} \\ \bar{\omega}_{2m} \end{cases} = \frac{\epsilon_m}{2\pi H_m} \int_0^{2\pi} (\bar{\zeta}_1 - \bar{\zeta}_A) \begin{cases} \cos m\theta \\ \sin m\theta \end{cases} d\theta \quad m = 0, 1, 2, \dots \quad (22)$$

Where H_m stands for $H_m^{(1)}(kR_2)$, R_2 being the radius of C_{12} .

The integral in (22) which involves $\bar{\zeta}_A$ can be determined exactly for any value of the integer m , since the integrand is expressed in terms of trigonometric functions. On the other hand, the integral which involves $\bar{\zeta}_1$ can only be determined approximately, as the latter function of θ is calculated only at a discrete set of points along C_{12} . Assuming that $\bar{\zeta}_1$ is given at N_2 equally spaced nodes on this boundary, we obtain:

$$\begin{cases} \bar{\omega}_{1m} \\ \bar{\omega}_{2m} \end{cases} = \frac{\epsilon_m}{N_2 H_m} \sum_{p=1}^{N_2} \bar{\zeta}_{1p} \begin{cases} \cos \Theta_{mp} \\ \sin \Theta_{mp} \end{cases} - a_0(i)^m \frac{\epsilon_m}{H_m} J_m(kR_2) \begin{cases} \cos m\alpha \\ \sin m\alpha \end{cases} \quad (23)$$

$$\Theta_n = 2\pi n / N_2$$

These expressions can also be derived by a direct identification of $\bar{\zeta}_2$ with $\bar{\zeta}_1$ at the N_2 points of the boundary C_{12} , and by applying a classical Fourier analysis.

It is known from the theory of spectral analysis that the sampling of the periodic function $\bar{\zeta}_1(\theta)$ at discrete points leads to a parasitic effect on the associated Fourier spectrum, so that it would be unrealistic to extend the application of (21) and (23) beyond a limiting value $m = N_2/2$. The order N of the finite series expansion used in practice is moreover dependent on the accuracy assigned in the numerical calculations. The latter criterion leads to a dependance of N on the value of the parameter kR_2 .

It is seen from (23) that $\bar{\zeta}_2$ and its normal derivative along C_{12} are linearly dependent on the value of $\bar{\zeta}_1$ at the N_2 nodes located on this boundary:

$$\bar{\zeta}_2 = \sum_{p=1}^{N_2} \lambda_{2p}(\theta) \bar{\zeta}_{1p} \quad M \in C_{12} \quad (24)$$

$$\frac{\partial \bar{\zeta}_2}{\partial n_2} = \sum_{p=1}^{N_2} \mu_{2p}(\theta) \bar{\zeta}_{1p} + \nu_2(\theta)$$

Calculations that will not be given in detail here, lead to the following expressions:

$$\lambda_{2p}(\theta) = \frac{1}{N_2} \sum_{m=0}^{N_S} \epsilon_m \cos m(\theta - \theta_p)$$

$$\mu_{2p}(\theta) = -\frac{k}{N_2} \sum_{m=0}^{N_S} \epsilon_m P_m(kR_2) \cos m(\theta - \theta_p) \quad (25)$$

$$\nu_2(\theta) = \frac{2a_0}{\pi R_2} \sum_{m=0}^{N_S} \frac{\epsilon_m}{H_m} (i)^{m+1} \cos m(\theta - \alpha)$$

$$P_m(u) = \frac{H_m^{(1)'}(u)}{H_m^{(1)}(u)}$$

where the prime stands for the first derivative of the function considered.

Within the domain D_1 , the problem is solved by a standard finite element technique. The solution and its spatial derivatives are represented by expressions of the form:

$$\bar{\zeta}_1(x, y) = \sum_n \gamma_n(x, y) \bar{\zeta}_{1n} \quad (26)$$

$$\frac{\partial \bar{\zeta}_1}{\partial x} = \sum_n \gamma_{xn} \bar{\zeta}_{1n} \quad ; \quad \frac{\partial \bar{\zeta}_1}{\partial y} = \sum_n \gamma_{yn} \bar{\zeta}_{1n}$$

where the summation extends over the whole set of finite elements, γ_n is an arbitrarily chosen interpolation function, depending on the type of discretisation and on the number of degrees of freedom within each element, and γ_{xn} , γ_{yn} are its spatial derivatives. Zero order continuity is generally sufficient for this class of partial differential equations.

By insertion of (24) and (26) into (17), we obtain:

$$F_c(\bar{\zeta}_1) = \sum_n \left[\sum_m A_{mn} \bar{\zeta}_{1m} \bar{\zeta}_{1n}^* + \sum_p B_{pn} \bar{\zeta}_{1p} \bar{\zeta}_{1n}^* + E_n \bar{\zeta}_{1n}^* \right] \quad (27)$$

$$A_{mn} = \iint_{D_1} \left[h(\gamma_{xm} \gamma_{xn} + \gamma_{ym} \gamma_{yn}) - \frac{\omega^2}{g} \gamma_m \gamma_n \right] ds \quad (28)$$

$$B_{pn} = \int_{C_{12}} h \mu_{2p} \lambda_{2n} d\sigma \quad ; \quad E_n = \int_{C_{12}} h \nu_2 \lambda_{2n} d\sigma$$

The summation with index m includes all finite elements which involve node n, and the summation with index p includes all nodes located on the boundary C₁₂, whenever node n is itself located on this boundary. The term E_n, as well, is involved only in the latter situation.

From the previous results, we obtain for the coefficients B_{pn} and E_n:

$$B_{pn} = - \frac{2\pi k R_2 h_0}{N_2} \sum_{m=0}^{N_s} \epsilon_m P_m(kR_2) \cos m(\Theta_p - \Theta_n) \quad (29)$$

$$E_n = \frac{4a_0 h_0}{N_2} \sum_{m=0}^{N_s} \frac{\epsilon_m}{H_m} (i)^{m+1} \cos m(\alpha - \Theta_n)$$

The conditions (20) then lead to the system of linear equations with N complex unknowns $\bar{\zeta}_{1n}$:

$$\sum_m A_{mn} \bar{\zeta}_{1m} + \sum_p B_{pn} \bar{\zeta}_{1p} = - E_n \quad n = 1, 2, \dots, N \quad (30)$$

The matrix of this system has a banded structure and symmetric coefficients, as can be seen from (28) for A_{mn} and (29) for B_{pn}. Moreover, all nodes which do not belong to the boundary C₁₂ are associated with real coefficients. Substantial savings in core memory requirements and in computer time are obtained by taking account of these properties in the implementation of the method.

SOLUTION FOR A SHORE-CONNECTED HARBOUR

In the case of a shore-connected harbour, with a rectilinear coastline bounding D₂, $\bar{\zeta}_D$ is an even function of Θ , which can be represented by (21) with only cosine terms present. The same method then gives:

$$\varpi_{1m} = \frac{\epsilon_m}{N_2 H_m} \sum_{p=0}^{N_2} \bar{\zeta}_{1p} \chi_p \cos \Theta_{mp} - 2a_0 (i)^m \frac{\epsilon_m}{H_m} J_m(kR_2) \cos m\alpha \quad (31)$$

$$\Theta_n = \pi n / N_2 \quad ; \quad \chi_p = \begin{cases} 0,5 & p = 0 \text{ or } N_2 \\ 1 & p = 1, 2, \dots, N_2 - 1 \end{cases}$$

For the reason indicated above, the order N of the finite Fourier series should not exceed the value $m = N_2$, assuming that $\bar{\zeta}_1$ is defined at N_2+1 nodes C_{12} . The formula (31) leads to expressions of $\bar{\zeta}_2$ and of its normal derivative along C_{12} which are similar to (24), with the index p starting from zero.

We thus obtain a system of linear equations similar to (30), with the coefficients specified in (28). The expressions of B_{pn} and E_n derived from (31) are:

$$B_{pn} = -\chi_p \chi_n \frac{\pi k R_2 h_0}{N_2} \sum_{m=0}^{N_s} \epsilon_m P_m(kR_2) \cos m \Theta_p \cos m \Theta_n \quad (32)$$

$$E_n = \frac{4a_0 h_0}{N_2} \chi_n \sum_{m=0}^{N_s} \frac{\epsilon_m}{H_m} (i)^{m+1} \cos m \alpha \cos m \Theta_n$$

The matrix of this system has the same general properties described for the preceding case.

FLOW AROUND THIN STRUCTURES

It is possible to account for the singularity of flow around the end of thin structures with the same method by introducing subdomains of circular shape D_3 at the tip, as shown in figure 1b. The functional F_c then involves additional integral expressions, in terms of N_3+1 unknown values of $\bar{\zeta}_1$ along the boundary C_{13} of these subdomains D_3 :

$$F_c(\bar{\zeta}) = \iint_{D_1} \left[h \nabla \bar{\zeta}_1 \cdot \nabla \bar{\zeta}_1^* - \frac{\omega^2}{g} \bar{\zeta}_1 \bar{\zeta}_1^* \right] ds + \int_{C_{12}} h \frac{\partial \bar{\zeta}_2}{\partial n_2} \bar{\zeta}_2^* d\sigma \quad (33)$$

$$+ \int_{C_{13}} h \frac{\partial \bar{\zeta}_3}{\partial n_3} \bar{\zeta}_3^* d\sigma$$

Since the solution of (3) within D_3 should have a finite value at the tip of the structure, its series expansion is of the form:

$$\bar{\zeta}_3(r, \psi) = \sum_{m=0}^{\infty} \rho_m J_{m/2}(kr) \cos \frac{m}{2} \psi \quad (34)$$

where (r, ψ) is here a local polar coordinate system, with its origin at the tip, and its reference axis aligned with the structure centerline, and $J_{m/2}$ is the Bessel function of fractional order $m/2$.

Along C_{13} , $\bar{\zeta}_3$ and its normal derivative take a form similar to (24).

Insertion of this into the last integral of (33) provides additional terms in (27) and finally leads to the following system:

$$\sum_m A_{mn} \bar{\delta}_{1m} + \sum_p B_{pn} \bar{\delta}_{1p} + \sum_q D_{qn} \bar{\delta}_{1q} = -E_n \quad n = 1, 2, \dots, N \quad (35)$$

with:

$$D_{qn} = \int_{C_{13}} h \mu_{3q} \lambda_{3n} d\sigma$$

$$D_{qn} = \chi_q \chi_n \frac{2\pi k R_3 h_3}{N_3^2} \sum_{m=0}^{N_3} \epsilon_m Q_m(kR_3) \cos \frac{m}{2} \psi_q \cos \frac{m}{2} \psi_n \quad (36)$$

$$Q_m(u) = J'_{m/2}(u) / J_{m/2}(u) \quad ; \quad \psi_n = 2\pi n / N_3$$

In (35), the summation with index q includes all nodes belonging to the boundary C₁₃, whenever node n is itself located on this boundary. The additional coefficients D^{qn} appearing in the matrix of the system are real and symmetric, as can be seen from (36). Thus, the inclusion of subdomains, such as D₃, within D₁ does not require any modification as concerns the numerical resolution of the system.

EXAMPLES OF APPLICATION

Several examples of application of the method will be given here. The first four cases are related to structures and harbours of simple geometry in constant water depth, for which results of other numerical methods and experimental investigations are available in the literature. The last example refers to an actual harbour project study, carried out by Sogreah, in which a complex harbour lay-out and a variable water depth are considered.

Wave diffraction by a circular cylinder

Figure 2a shows the finite element numerical model adopted for the analysis of the wave diffraction pattern around a cylindrical structure of circular shape, of radius R₀, subject to a plane incident wave.

The variation of the calculated relative wave height along the cylinder, for different values of the adimensional parameter kR₀, is shown in figure 3, where it is compared to the analytical solution of Mac Camy and Fuchs [7]. The agreement between both methods is satisfactory.

Figure 4a gives for kR₀=1, the spatial distribution of the relative wave height in the whole domain D₁, in the form of level curves.

Figure 4b gives the corresponding water surface level, at the instant of maximum elevation at the most exposed part of the cylinder. In the same

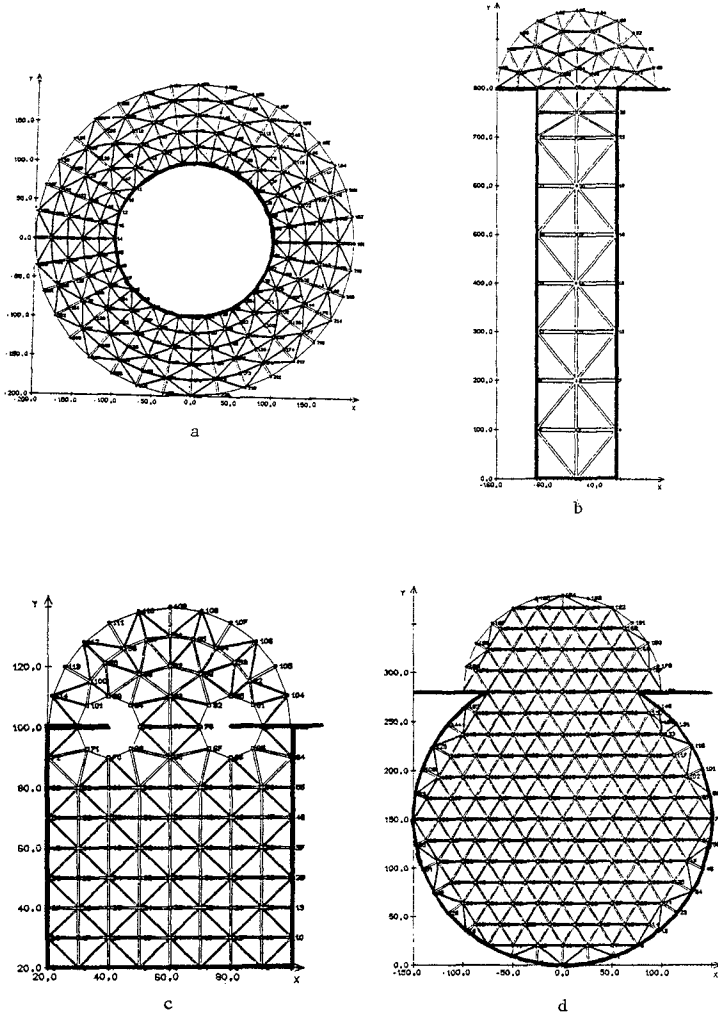


Fig. 2 Numerical models for : (a) a vertical circular cylinder, (b) a rectangular harbour $b/L = 0.2$, (c) a partially closed square harbour $w/b = 0.5$, (d) a circular harbour with 60° opening.

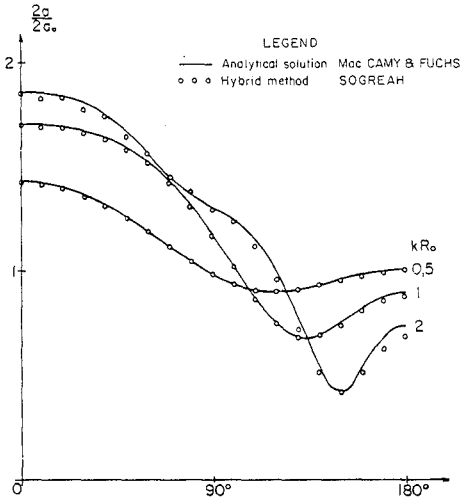


Fig. 3 Wave diffraction by a circular cylinder. Wave-height distribution along the structure for different values of kR_0 .

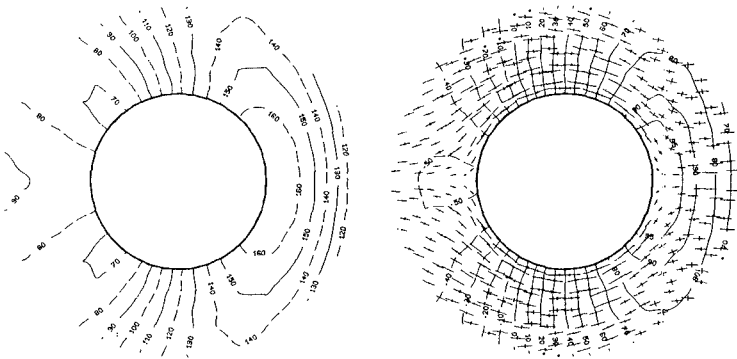


Fig. 4 Spatial distribution of the amplification coefficients (left), water surface elevation and horizontal displacements (right) for $kR_0 = 1$.

Fig 5 CALCULATION OF SEICHE MOTIONS IN A RECTANGULAR HARBOUR WITH $B/L=0.2$

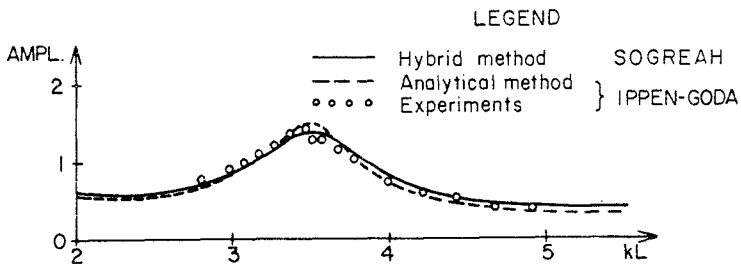
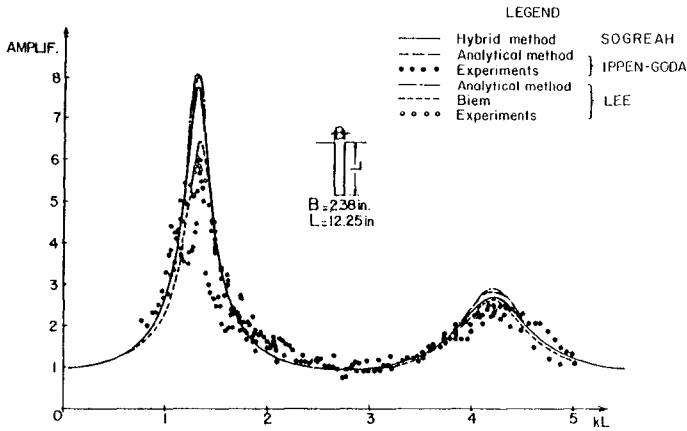


Fig. 6 Calculation of seiche motions in a partially closed square harbour with $D/B = 0.5$. Amplification at back wall.

figure are given the direction and length of the major and minor axes of the water particle horizontal displacements and hodographs, which are generally of elliptical form, as shown by the author in [4].

Seiche motions in a rectangular harbour

The second example is the study of resonant wave oscillations in a shore-connected rectangular harbour, with a width to length ratio $W/L=0.2$, and fully open on its narrow side, as shown in figure 2b. This situation was studied both experimentally and theoretically by Ippen and Goda [5], and by Lee [6], with a ratio $W/L=0.193$.

Figure 5 gives the frequency response obtained by these various approaches at the back wall of the harbour. The results obtained by the present method agree well with Ippen and Goda's and Lee's analytical solutions, which take explicitly account of the rectangular shape of the harbour. The results obtained by Bettess and Zienkiewicz [2] and by Chen and Mei [3], which are not shown here, also agree with the above results.

The experimental results and Lee's arbitrary shaped harbour theory, based on a boundary integral approach, agree with the other methods for the second mode of resonance, but give a noticeably lower amplification factor for the first mode. Ippen and Goda suggest that this could be due to energy dissipation, since experiments were actually performed with short waves of high steepness. It has not been investigated whether a refinement of the finite element network would improve the agreement with those experimental results.

Case of a partially closed square harbour

The case of a square harbour, partially closed by two thin aligned breakwaters, is given for illustrating the use of circular subdomains D_3 around the tip of harbour structures, as shown in figure 2c.

Figure 6 compares the numerical results obtained by the present method with Ippen and Goda's analytical solution and with their experimental results for an entrance width to harbour length ratio $W/L=0.5$. The agreement between the different methods is very close.

Case of a circular harbour

The case of a shore-connected circular harbour with a 60° opening is an application involving more complex resonant nodes, which has been investigated both experimentally and theoretically by Lee [6].

Figure 7 gives the frequency response calculated at two different locations with the numerical model shown in figure 2d, together with the results of Lee's investigation.

Figure 8 shows the features of the first four resonant modes, which are obtained for $kR_0=0.51, 2.21, 3.43$ and 4.09 approximately, with the present method. The water surface elevation is indicated by means of level curves,

Fig. 7a CALCULATION OF SEICHE MOTIONS IN A CIRCULAR HARBOUR WITH A 60° OPENING
AMPLIFICATION COEFFICIENT AT POINT A ($r/R_0 = 0.933 - \theta = 45^\circ$)

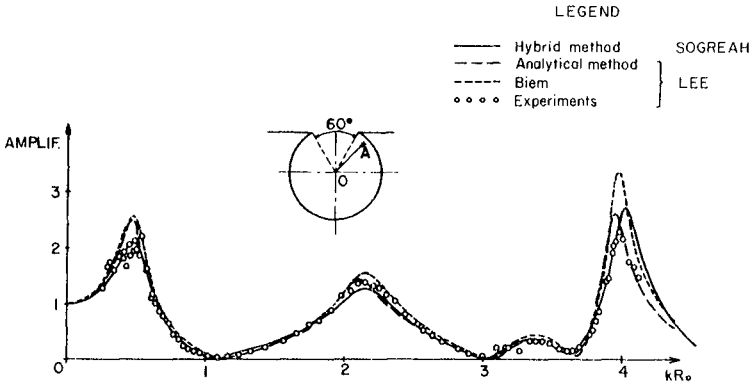
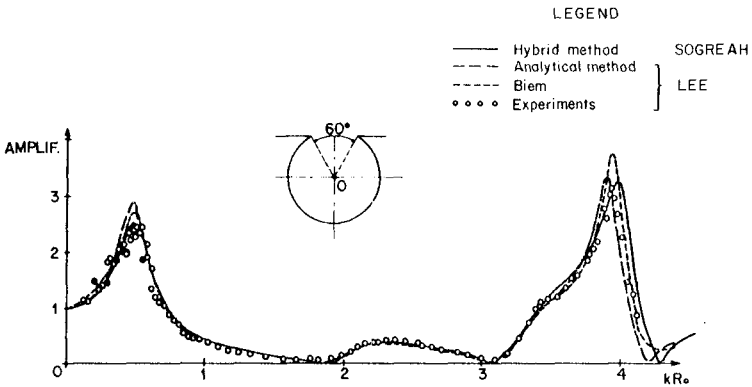


Fig. 7b CALCULATION OF SEICHE MOTIONS IN A CIRCULAR HARBOUR WITH A 60° OPENING
AMPLIFICATION COEFFICIENT AT CENTER O



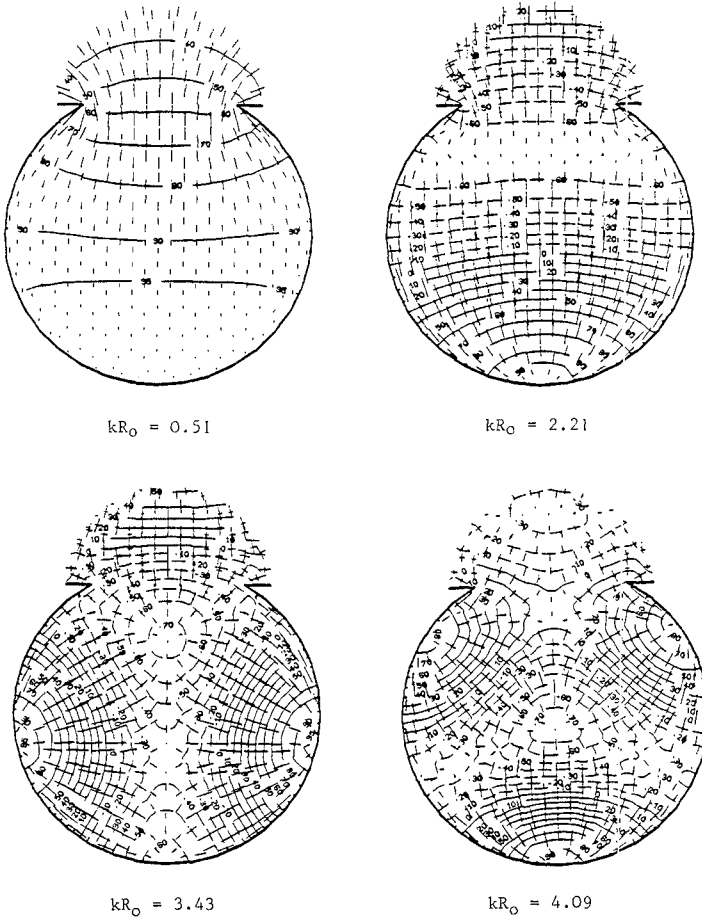


Fig. 8 Water surface elevation and horizontal displacements for the first resonant modes of a circular harbour with a 60° opening.

corresponding to given percentages of the maximum elevation. The instant taken as reference is that of maximum elevation at the point of highest amplification.

The direction and length of the major and minor axes of the horizontal water particle displacements and velocities are given on the same figure at the centroid of each finite element. The wave motion has essentially the character of purely standing waves in a great part of the harbour, and the water particles horizontal motion is practically rectilinear and oriented in the direction of the local amplitude gradient. This is not the case for particles located near the entrance, either within or outside the harbour, which have elliptical horizontal trajectories.

The resonant modes calculated by Lee are similar to the above. From the frequency response curve of the mean velocity at the harbour entrance, the values of kR_0 corresponding to resonance were found by Lee, to be 0.50, 2.18, 3.38 and 3.97. These figures agree to within 3% with these of the present model.

Case of a harbour of complex shape and variable water depth

Because of accuracy requirements, the maximum size of the finite elements should stay below a certain fraction of the local wave length, which depends on the type of spatial discretisation and interpolation functions used for ζ . With triangular elements and linear interpolation, for instance, this limit is of the order of 0.1. In the case of a harbour of variable water depth, the size of the finite elements will thus be dependent on the distribution of water depths to be considered.

Figure 9 is an example of application of the method to a harbour of complex shape and bottom topography (from 2 m to 15 m below MSL), with two main breakwaters extending offshore to protect the entrance channel. This model was set up for the study of the new Damietta Port Project in Egypt.

Figure 10 shows the frequency response curve obtained for one of the reference calculation points, which displays a great number of resonance frequencies. An in-depth investigation of each resonant mode was carried out on the basis of such results.

Figure 11 shows the features of one of the resonant modes of this harbour, in the form described for the circular harbour, i.e., level curves of water surface elevation and major and minor axis length and direction of horizontal water motion.

CONCLUSION

The present method leads to a system of linear equations, with symmetric coefficients, in which the only unknowns are the values of the complex function ζ at nodes distributed within the bounded domain D_1 , and along its boundary. In the other hybrid-element methods a larger system is obtained with additional unknowns, which are the Fourier coefficients α_m , α_m^2 , in Chen and Mei's method, the normal derivatives in Sakaï and Tsukioka's method, the source strengths in Berkhoff's method, and the ζ_1 , or velocity potential values, at nodes distributed along infinite elements in Bettess and Zienkiewicz's method.

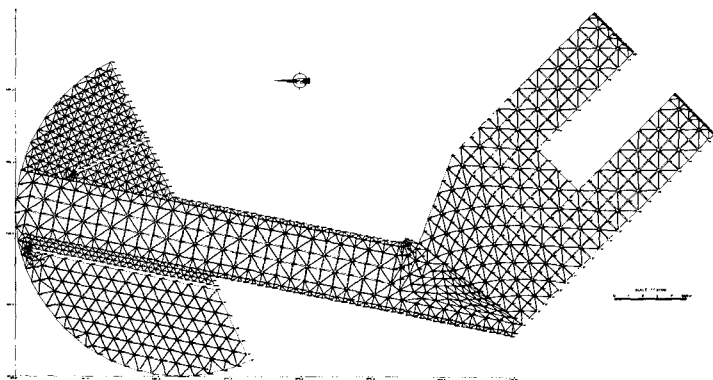


Fig. 9 - Numerical model set up for the study of seiche motions in the new Damietta industrial harbour (Egypt).

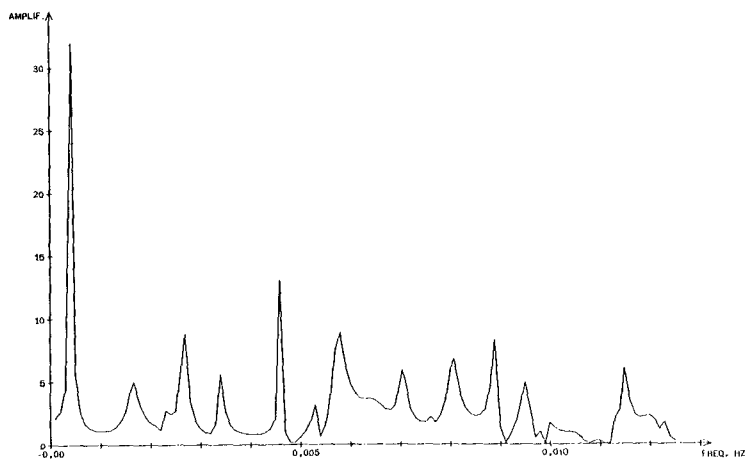


Fig. 10 - Frequency response curve at one of the reference nodes of the Damietta harbour model

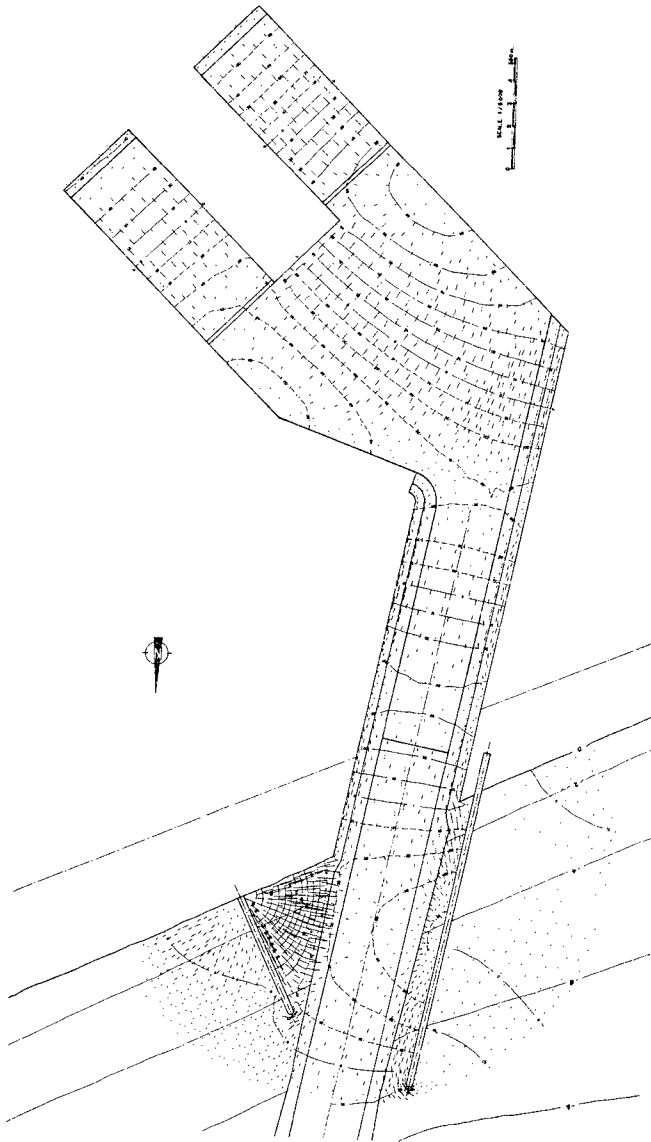


Fig. 11 - Water surface elevation and horizontal displacements for one of the resonant modes of the Damietta harbour model.

The present method is based on the same analytical representation of ζ in the outer domain D_2 , as in Chen and Mei's approach. However, here an explicit formulation of w_{1m} , w_{2m} in terms of the incident wave characteristics and of the unknown values of $\bar{\zeta}_1$ along C_{12} , is given. This method is preferable to the matrix inversion technique used by the above authors. Another advantage of the method is the simplicity of form of the functional $F_c(\bar{\zeta})$ involved in (17) and (33), as compared to Chen and Mei's formulation.

The method, presented here in connection with studies of long wave oscillations in harbours, can be applied, with only minor changes as concerns the treatment of domain D_1 , to the study of wave oscillations in the short and intermediate period range. It can also be extended to include energy dissipation and partial reflection along the shore and harbour structures.

The application of the present method to various situations for which other theoretical and experimental investigations have been carried out, has led to numerical results in good agreement with the above methods.

REFERENCES

- [1] BERKHOFF J.C.W. (1972) "Computation of combined refraction-diffraction" Proc. 13th Int. Coastal Engineering Conf. Vol. 2, p. 471-490.
- [2] BETTESS P & ZIENKIEWICZ O.C. (1977) "Diffraction and refraction of surface waves using finite and infinite elements" Int. journal for numerical methods in Engineering, vol. 11, p. 1271-1290.
- [3] CHEN H.S. & MEI C.C. (1974) "Oscillations and wave forces in an offshore harbour. Application of hybrid finite element method to water wave scattering" M.I.T. Rep. No. 190, Ralph Parsons Lab. for Water Resources and Hydrodynamics.
- [4] CAILLARD P. (1982) "Kinematic and dynamic properties of diffracted waves in constant water depth". In Engineering applications of Computational Hydraulics. Homage to Alexandre PREISSMANN, Vol. 1., Pitman Publ., p. 131-183.
- [5] IPPEN A.T. & CODA Y. (1963) "Wave induced oscillations in harbours: The Solution for a rectangular harbour connected to the open-sea" Hydrodynamics Lab., Massachusetts Inst of Technology, Rep. No. 59.
- [6] LEE J.J. (1969) "Wave induced oscillations in harbours of arbitrary shape" W.M. KECK Lab. of Hydraulics and Water Resources. California Inst. of Technology, No. KH-R-20.
- [7] MAC CAMY R.C. & FUCHS R.A. (1952) "Wave forces on piles: a diffraction theory". Inst. Engineering Research. Waves Investigation Lab., Series 3, Issue 334, Berkeley, Calif.
- [8] SAKAI F & TSUKIOKA K. (1976) "Finite element simulation of surface wave problems". Proc. 1rst Int. Conf. on Finite Elements in Water Resources. Princeton Univ., p. 4.3-4.17.